DOI: 10.19884/j.1672-5220.202308003

Suppressing Leakage Currents and Improving Performance of Indoor Organic Photovoltaic Devices

WANG Xiang, GAO Jiaxin, LI Zheng, WANG Ming*, TANG Zheng*
State Key Laboratory for Modification of Chemical Fibers and Polymer Materials, Center for Advanced Low-dimension Materials, College of Materials Science and Engineering, Donghua University, Shanghai 201620, China

Abstract: Organic photovoltaic (OPV) devices hold great promise for indoor light harvesting, offering a theoretical upper limit of power conversion efficiency that surpasses that of other photovoltaic technologies. However, the presence of high leakage currents in OPV devices commonly constrains their effective performance under indoor conditions. In this study, we identified that the origin of the high leakage currents in OPV devices lay in pinhole defects present within the active layer (AL). By integrating an automated spin-coating strategy with sequential deposition processes, we achieved the compactness of the AL and minimized the occurrence of pinhole defects therein. Experimental findings demonstrated that with an increase in the number of deposition cycles, the density of pinhole defects in the AL underwent a marked reduction. Consequently, the leakage current experienced a substantial decrease by several orders of magnitude which achieved through well-calibrated AL deposition procedures. This enabled a twofold enhancement in the power conversion efficiency (PCE) of the OPV devices under conditions of indoor illumination.

Key words: organic photovoltaic (OPV); indoor light harvesting; pinhole defect; leakage current; shunt resistance
CLC number: TB34 **Document code**: A
Article ID: 1672-5220(2024)04-0388-10

Open Science Identity (OSID)

0 Introduction

Organic photovoltaic (OPV) technology has significant potential for development in the field of renewable energy due to its advantages such as simple fabrication processes, low cost, flexibility and foldability[1-8]. In particular, OPV technology exhibits excellent photovoltaic performance under weak indoor light conditions, with theoretical power conversion efficiencies (PCEs) over 50%[9-13]. This characteristic makes OPV devices the optimal choice for passive power supply in indoor electronic devices, thereby driving the advancement of emerging electronic technology fields including the Internet of Things (IoT)[13-18].

The potential of indoor light OPV devices far surpasses that of inorganic photovoltaic devices, and this can be attributed to the unique properties of OPV materials[18-20]. Under weak indoor light conditions, inorganic photovoltaic devices generate lower concentrations of charge carriers[21-22]. At such conditions, charge carriers experience significant surface and interface recombination within the inorganic semiconductor, due to the presence of high density of defects in inorganic materials, which greatly limits the indoor photovoltaic performance of the devices. In contrast, organic semiconductor materials have fewer surface and interface defects[18,23-24]. Therefore, under weak light conditions, the photo-generated free carriers in OPV devices can still be efficiently collected by the electrodes, resulting in exceptional photovoltaic performance. Additionally, of greater importance is the ability of organic semiconductor materials to be optically designed specifically for indoor light-emitting diode (LED) spectra[25-28]. This enables the matching of the absorption spectrum of the organic photoactive layer with the emission spectrum of the LED, further enhancing the photovoltaic performance of OPV devices under indoor LED illumination.

Although indoor light OPV devices have the aforementioned advantages, the devices suffer from higher leakage currents due to their thin active layer (AL), which is only a few tens of nanometers thick. While such leakage issues have a minor impact on the performance of outdoor OPV devices[29-31], they severely limit the performance of the devices under indoor weak light conditions. Therefore, the leakage issue is crucial in determining the indoor light performance of OPV devices. The reason for the high leakage current in OPV devices lies in the presence of numerous pinhole defects in the AL prepared by solution processing[30,32]. These defects make it easier for the anode and cathode of the device to come into direct contact, resulting in a small shunt resistance R_{sh} and a high leakage current[29,32].

Received date: 2023-08-25
Foundation item: Fundamental Research Funds for the Central Universities, China (No. 2232022A13)
* Correspondence should be addressed to WANG Ming, email: mwang@dhu.edu.cn; TANG Zheng, email: ztang@dhu.edu.cn
Citation: WANG X, GAO J X, LI Z, et al. Suppressing leakage currents and improving performance of indoor organic photovoltaic devices [J]. *Journal of Donghua University (English Edition)*, 2024, 41(4): 388-397.

Since the density and random distribution of pinhole defects in the AL are significant, this also leads to poor reproducibility of the photovoltaic performance of indoor OPV devices under weak light conditions[33-34]. For OPV devices, the generation of pinhole defects mainly stems from the complex dynamics of the solution-coating process. To address this issue, new deposition strategies need to be developed to suppress the probability of pinhole defect occurrence and its impact on device leakage current.

In this work, we improved the reproducibility of solution-processed organic ALs by developing an automated spin-coating strategy. By combining the automated spin-coating strategy with sequential deposition processes, we significantly enhanced the compactness of the AL and reduced the density of pinhole defects in the AL. Experimental results showed that as the number of depositions increased, the density of pinhole defects in the AL decreased significantly. When the number of depositions exceeded three, no apparent pinhole defects were observed in the AL, leading to an increase in R_{sh} of the devices with an increasing number of depositions. Thus, the automated sequential deposition strategy greatly improved the performance of the devices under weak indoor light conditions. These results emphasize the significance of AL processing conditions in suppressing device leakage current, thereby enhancing the performance of indoor OPV devices.

1 Materials and Methods

1.1 Materials

Polymer donor PM6 (poly[(2, 6-(4, 8-bis(5-(2-ethylhexyl-3-fluoro)thiophen-2-yl)-benzo[1, 2-b:4, 5-b']dithiophene))-alt-(5, 5-(1′, 3′-di-2-thienyl-5′, 7′-bis(2-ethylhexyl)benzo[1′, 2′-c:4′, 5′-c′]dithiophene-4, 8-dione)]) was synthesized following the method reported in Ref. [35]. The non-fullerene electron acceptor Y6 (2, 2′-((2Z, 2′Z)-((12, 13-bis(2-ethylhexyl)-3, 9-diundecyl-12, 13-dihydro-[1, 2, 5]-thiadiazolo[3, 4-e]-thieno[2″, 3″: 4′, 5′]thieno-[2′, 3′: 4, 5]pyrrolo-[3, 2-g]thieno-[2′, 3′:4, 5]thieno-[3, 2-b]indole-2, 10-diyl)bis(methanylylidene))bis(5, 6-difluoro-3-oxo-2, 3-dihydro-1H-indene-2, 1-diylidene))dimalononitrile) was purchased from Suna Tech. Inc., China. 1-Chloronaphthalene, chloroform and other routine chemicals were purchased from Sigma-Aldrich, China.

1.2 Device fabrication

The OPV devices in this work were fabricated using an indium tin oxide (ITO)-free device architecture of glass/Ti (2 nm)-Al (100 nm)-Ti (2 nm)/PM6∶Y6/MoO_3(10 nm)/Ag (5 nm). The glass substrates were firstly cleaned using TL-1 for 40 min at 90 ℃, where TL-1 was the mixture of $NH_3 \cdot H_2O$ (mass fraction: 25%), H_2O_2(mass fraction: 30%) and ultra-pure water in a volume ratio of 1∶1∶5. The Ti-Al-Ti multilayer electrode was successively deposited through a shadow mask under a vacuum pressure of 2×10^{-4} Pa. The PM6∶Y6 solution was prepared utilizing chloroform as host solvent mixed with 1-chloronaphthalene in a volume fraction of 0.5% as an additive. The mass ratio of the donor PM6 to the acceptor Y6 was 1∶1.2. The mass concentrations of the active materials were 16, 12, 10, 8, 6 and 4 mg/mL in total for the ALs obtained from 1, 2, 3, 4, 5 and 15 spin-coating times, respectively. The ALs were deposited on top of the Ti-Al-Ti coated glass substrates by spin-coating method with a spin speed of 3 000 r/min. The thicknesses for all the ALs were about 100 nm. After that, the substrates were transferred into a vacuum chamber located in a glove box filled with nitrogen. Finally, MoO_3 (10 nm) and Ag (5 nm) layers were deposited under a vacuum pressure of 2×10^{-4} Pa through a shadow mask. The active area for the OPV devices was 0.04 cm^2.

1.3 Device characterizations

The current density-voltage (*J-V*) curves were recorded with a Keithley 2450 source meter (Tektronix, USA) under different illumination conditions. For the outdoor performance of the OPV devices, a simulated solar illumination (100 mW/cm^2, AM 1.5 G) from a solar simulator (Newport-Oriel® Sol, class AAA, USA) was used as the illumination source. The indoor photovoltaic performance of the OPV devices was determined using a white LED lamp (6 500 K) as the illumination, the spectral of the LED lamp was calibrated by a spectrometer (KYMERA-328I-B2, coupled with a charge-coupled device (CCD) camera, DU970P-BVF, Andor, UK), with the spectral irradiance varied by using neutral density filters.

External quantum efficiency (EQE) spectra were obtained using a homebuilding setup, with a halogen lamp (150W, LSP-T75, Newport, UK), an optical chopper (Newport, USA), a monochromator (CS260-RG-3-MC-A, Newport, USA) and a pre-current amplifier (Model SR570, Stanford, USA).

Ultraviolet-visible-near infrared (UV-Vis-NIR) spectroscopy absorption spectra were determined with a UV-Vis-NIR spectrophotometer (Lambda 950, PerkinElmer, USA).

The AL thicknesses were recorded by a profilometer (Tensor P-7 Stylus Profiler, KLA, USA).

Atomic force microscopy (AFM) images were determined using an Agilent 5500 instrument (Agilent Technologies, Inc., USA) in a tapping mode.

Reflectance microscope images of the AL thin films were measured with an LV100NPOL/Ci-POL (Nikon, Japan).

2 Results and Discussion

2.1 Performance of OPV devices constructed by manual and automated spin-coating process

In order to investigate the influence of the manual

spin-coating process on the performance of OPV devices, we employed the PM6∶Y6 system[36], a classic commercially available donor-acceptor system, as the AL in our study. The chemical structures of these active materials are depicted in Fig. 1(a), while their electrochemical and optical properties are shown in Figs. 1(b) and 1(c), respectively. We fabricated ITO-free devices using an inverted structure with the following device architecture: glass/Ti/Al/Ti/AL/MoO_3/Ag[37]. Initially, a solution of PM6∶Y6 with a mass concentration of 16 mg/mL in chloroform was manually spin-coated onto the Al-Ti substrate electrode. Subsequently, MoO_3 (10 nm) and Ag (5 nm) were deposited onto the AL to complete the fabrication of the OPV devices. A total of 20 sets of devices were prepared under the same conditions.

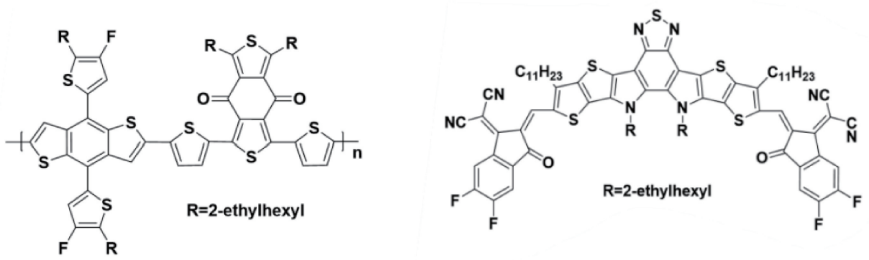

Donor: PM6 Acceptor: Y6

(a)

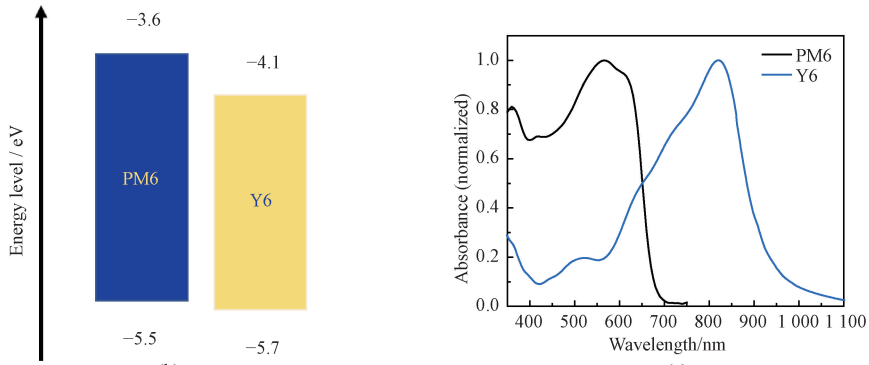

(b) (c)

Fig. 1 Material characterizations: (a) chemical structures of donor and acceptor materials; (b) energy levels of active materials; (c) UV-Vis-NIR absorption spectra of thin films based on pure PM6 and pure Y6

The dark *J-V* curves of these devices were measured, as shown in Fig. 2(a). Next, the R_{sh} values of the devices were calculated, and the dark current density values at a bias of −0.5 V, referred to as the leakage current density J_{leak} of the devices, were obtained. Subsequently, the R_{sh} and J_{leak} values for the 20 sets of devices were plotted in Fig. 2(b). From Figs. 2(a) and 2(b), it can be observed that the R_{sh} values of the OPV devices obtained via the manual spin-coating method are quite dispersed, ranging from 0.3 to 354.9 kΩ/cm^2, with relatively low values and an average of approximately 10 kΩ/cm^2. Similarly, the J_{leak} values of the devices also exhibit significant dispersion, ranging from 7.5×10^{-3} to 34.8 mA/cm^2 for the 20 sets of devices at −0.5 V. Due to the small R_{sh} values, the devices exhibit high leakage current, with an average J_{leak} of 0.5 mA/cm^2. For representative OPV devices with an average R_{sh}, the *J-V* curves were measured under the AM1.5 (100 mW/cm^2) illumination condition and different LED (6 500 K) illumination intensities. The results are presented in Fig. 2(c) and Table 1. It can be observed that under the AM1.5 illumination condition, the device exhibits a short-current density J_{sc} of 19.26 mA/cm^2, open-circuit voltage V_{oc} of 0.84 V, fill-factor (FF) of 69.0%, and PCE of 11.21%, which are decent, compared to that reported in the literature. However, under LED (6 500 K) illumination conditions with an intensity of 10 000 lux (light intensity P_{in} = 3.34 mW/cm^2), the device's PCE decreases to 8.22%. This is primarily attributed to the increased leakage current, leading to significant reductions in V_{oc} and FF under weak light conditions. Further reduction of the LED intensity to 2 000 lux results in a decrease in V_{oc} and FF to 0.33 V and 32%, respectively, with a PCE of only 2.76%.

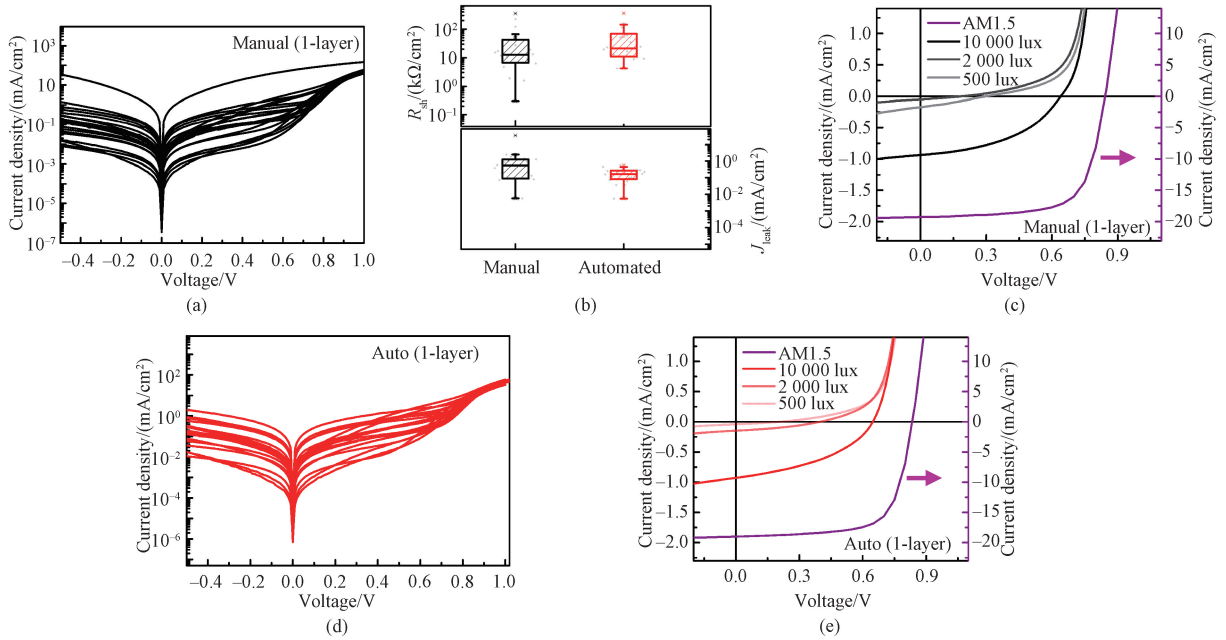

Fig. 2 PM6∶Y6 based OPV device performance and fabrication method comparison: (a) dark *J-V* curves of the devices employing the manual spin-coating fabrication method; (b) R_{sh} and J_{leak} at −0.5 V across a set of 20 devices fabricated using both manual and automated spin-coating methods; (c) *J-V* curves of the devices manufactured through the manual spin-coating method; (d) dark *J-V* curves of the devices employing the automated spin-coating fabrication method; (e) *J-V* curves obtained with different light sources of the OPV devices fabricated by automated spin-coating method

In order to reduce the dispersion of device R_{sh} and leakage current and facilitate the identification of experimental methods for reducing device leakage current, we employed an automated spin-coating method to fabricate the AL of the devices. In the automated spin-coating process, the solution of the active material is automatically dispensed at a constant rate from a highly fixed syringe onto a substrate that is spinning at a specific rotational speed. The thickness of the AL is controlled by adjusting the solution concentration and substrate rotation speed. By regulating the injection speed and height of the solution, the macroscopic reproducibility of the active thin film is controlled. After optimizing the processing parameters of the automated spin coater, we deposited a solution of PM6∶Y6 with a mass concentration of 16 mg/mL in chloroform as the AL to fabricate ITO-free OPV devices. Similarly, 20 sets of devices prepared under the same conditions were subjected to dark *J-V* curve testing, as shown in Fig. 2(d). The statistical results for R_{sh} and J_{leak} are presented in Fig. 2(b). From the statistical results of R_{sh} and J_{leak}, it can be observed that the dispersion of R_{sh} and J_{leak} values for the devices fabricated using automated spin-coating is significantly lower compared to those obtained from manual spin-coating of OPV devices. The R_{sh} values of the devices fabricated via automated spin-coating are within the range of 9.2 to 359.6 kΩ/cm^2, while the corresponding J_{leak} values are within the range of 5.5×10^{-3} to 0.58 mA/cm^2. It is worth noting that, compared to the manual spin-coating process, the automated spin-coating strategy also alleviates the leakage problem of the devices. The average R_{sh} of the devices fabricated via automated spin-coating increased to 20 kΩ/cm^2, while the average J_{leak} was 0.1 mA/cm^2.

Then, we tested the *J-V* curves of the devices with R_{sh} at the average level under different illumination conditions. As shown in Fig. 2(e) and Table 1, under AM1.5 illumination condition, the devices exhibited performance consistent with those fabricated using manual spin-coating, with a PCE of about 11%. This result further indicates that the magnitude of the leakage current has no significant impact on the device's performance under strong illumination conditions. However, the devices obtained through automated spin-coating still exhibit relatively large J_{leak}, which should limit their performance under weak light conditions. Indeed, under LED (6500 K) illumination conditions, when the light intensity is 10000 lux, the device's PCE decreases to 8.41%. This indicates that although the automated spin-coating strategy can significantly reduce the dispersion of device R_{sh} and J_{leak}, it does not significantly improve the photovoltaic performance of OPV devices under weak light conditions.

Table 1 Representative photovoltaic performance parameters for the OPV devices based on PM6∶Y6 fabricated by manual or automated spin-coating method

Method	Light source	Intensity/lux	Power/(mW/cm^2)	J_{sc}/(mA/cm^2)	V_{oc}/V	FF/%	PCE/%
Manual	AM1.5	213 000	100.000	19.260	0.840	69.0	11.21
	LED	10 000	3.340	0.940	0.646	45.4	8.22
	LED	2 000	0.668	0.180	0.329	32.0	2.76
	LED	500	0.167	0.048	0.190	28.7	1.58
Automated (1 layer)	AM1.5	213 000	100.000	19.020	0.834	69.2	10.97
	LED	10 000	3.340	0.930	0.652	46.4	8.41
	LED	2 000	0.668	0.150	0.401	34.2	3.00
	LED	500	0.167	0.040	0.206	29.0	1.44
Automated (2 layers)	AM1.5	213 000	100.000	19.300	0.830	69.7	11.20
	LED	10 000	3.340	0.930	0.716	54.3	10.85
	LED	2 000	0.668	0.190	0.542	40.3	6.08
	LED	500	0.167	0.035	0.312	35.4	2.29
Automated (5 layers)	AM1.5	213 000	100.000	19.360	0.836	70.0	11.33
	LED	10 000	3.340	1.000	0.739	70.6	15.57
	LED	2 000	0.668	0.200	0.656	62.4	12.43
	LED	500	0.167	0.050	0.614	53.1	9.72
Automated (15 layers)	AM1.5	213 000	100.000	19.140	0.835	70.8	11.41
	LED	10 000	3.340	0.940	0.735	70.2	14.58
	LED	2 000	0.668	0.180	0.657	62.2	10.93
	LED	500	0.167	0.043	0.566	51.7	7.57

To identify the reasons for the large J_{leak} in the devices, we characterized the distribution of pinhole defects in the ALs using reflectance microscopy, as shown in Figs. 3(a) and 3(b). It can be observed that both the manual and automated spin-coating ALs exhibit a high density of pinhole defects. Consequently, the positive and negative electrodes of the devices directly contact each other through these pinhole defects, causing short circuits and resulting in device leakage. By analyzing the reflective microscopy images, we found that the proportionate area of pinhole defects in the ALs reached as high as 11%. In order to enhance the device's performance under indoor light conditions, further development of experimental methods that can reduce pinhole defects and device leakage current is necessary.

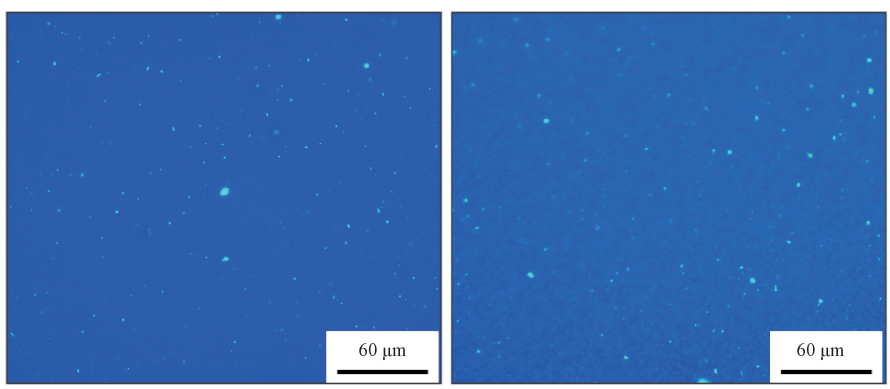

Fig. 3 Reflectance images of PM6∶Y6 AL thin films prepared in different methods: (a) manual spin-coating; (b) automated spin-coating

2.2 Impact of sequential deposition strategy on the performance of OPV devices fabricated using automated spin-coating method

To address the aforementioned pinhole issues, we developed a sequential deposition process for the AL. The proposal of this experimental strategy is primarily based on the hypothesis that pinhole defects originate from the dewetting during the drying process of the AL. Using the sequential deposition strategy, we aimed to reduce the density of pinhole defects in the AL obtained from a one-time deposition by depositing the AL multiple times. This, in turn, would reduce device leakage current and enhance the photovoltaic performance of the devices under weak light conditions.

Initially, we investigated the photovoltaic performance of devices based on a two-time automated spin-coating approach. To ensure consistent AL thickness, the mass concentration of the active material solution was reduced to 10 mg/mL. More specifically, the solution was spin-coated to form the AL, and another layer of the active material was spin-coated on top of the previously deposited AL using the same conditions. The total thickness of the AL reached 100 nm after the two spin-coating steps. We then examined the optical microscopy and AFM images of the ALs processed with one- and two-time spin-coatings. The reflectance images and AFM height images are shown in Fig. 4 and the proportionate area P of pinhole defects in the ALs was indicated in the images.

As shown in Fig. 4, compared to the AL obtained from a single spin-coating, the density of pinhole defects in the AL obtained from two consecutive spin-coatings was significantly reduced, aligning with our previous expectations.

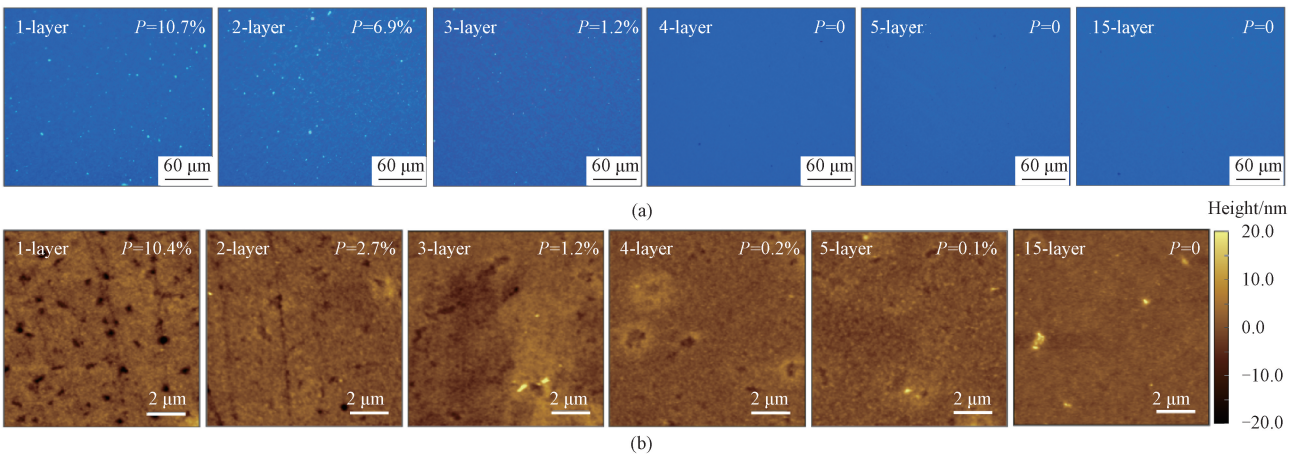

Fig. 4 Morphology of PM6∶Y6 AL thin films obtained utilizing automated spin-coating method: (a) reflectance images; (b) AFM height images

Subsequently, we tested the dark J-V curves of the devices, as shown in Fig. 5(a). Similarly, we selected 20 sets of device J-V curves for data analysis of R_{sh} and J_{leak}, as presented in Figs. 6(a) and 6(b). The test results demonstrate that after two consecutive spin-coatings of the AL, the dispersion of R_{sh} and J_{leak} values significantly decreased due to the noticeable reduction in pinhole defects within the AL. The range of R_{sh} was 37.4–510.9 kΩ/cm^2, with corresponding J_{leak} values ranging from 8.7×10^{-3} mA/cm^2 to 0.19 mA/cm^2. Additionally, compared to devices based on a single spin-coating AL, the two-time spin-coating of the AL led to a significant increase in R_{sh}, with an average value of 200 kΩ/cm^2. Consequently, the J_{leak} of the devices obtained after the two spin-coatings was notably suppressed, with the average J_{leak} being only 10% of that obtained from devices with a single spin-coated AL.

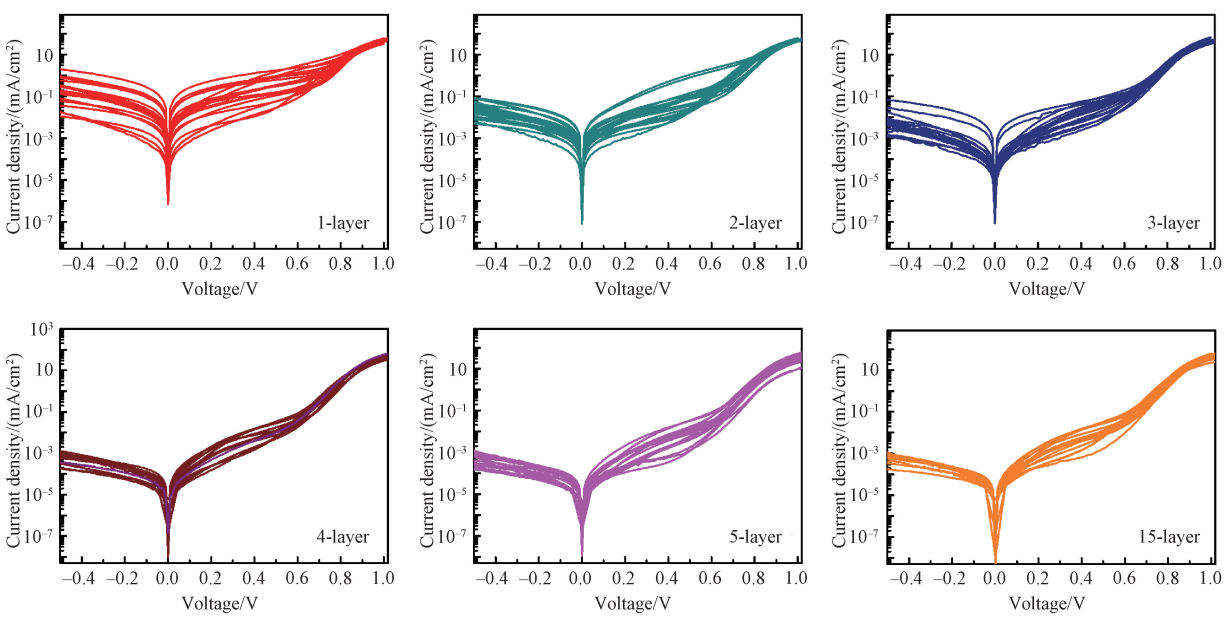

Fig. 5 Dark J-V curves for PM6∶Y6 based OPV devices with varying AL deposition times

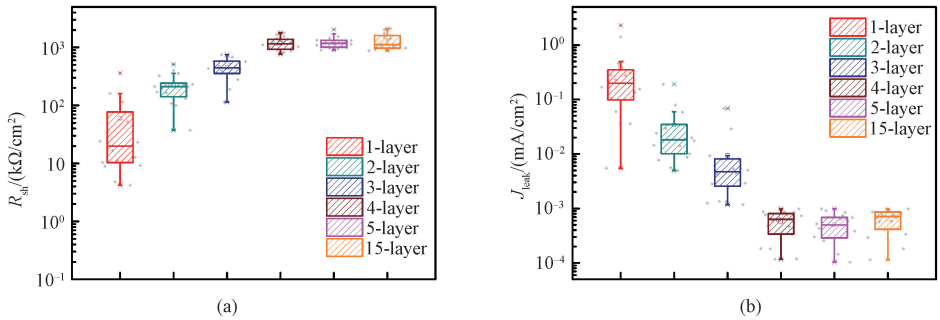

Fig. 6 Electrical characteristics of PM6∶Y6 based OPV devices fabricated via automated spin-coating: (a) R_{sh}; (b) J_{leak} at −0.5 V observed in a set of 20 devices based on the PM6∶Y6 blend

To investigate the impact of two consecutive spin-coatings of the AL on the photovoltaic performance of the devices under weak light conditions, we also tested the *J-V* curves of the devices under different LED (6 500 K) illumination intensities. The results are shown in Fig. 7(a), and the photovoltaic performance parameters are summarized in Table 1. It can be observed that with the AL processed with two spin-coatings, the OPV devices exhibited better photovoltaic performance. When the light intensity was 10 000 lux, the devices achieved a V_{oc} of 0.716 V, an FF of 54.3% and a corresponding PCE of 10.85%. Furthermore, when the light intensity was further reduced to 2 000 lux, the device's PCE reached 6.08%, with a V_{oc} of 0.542 V and an FF of 40.3%. These values were significantly higher than the photovoltaic performance of the OPV devices with the AL processed with one-time spin-coating, under the same illumination conditions. However, it is worth noting that even in the AL processed with two-time spin-coating, pinhole defects can still be observed, and the photovoltaic performance of the devices is still limited when the light intensity is further decreased to 500 lux.

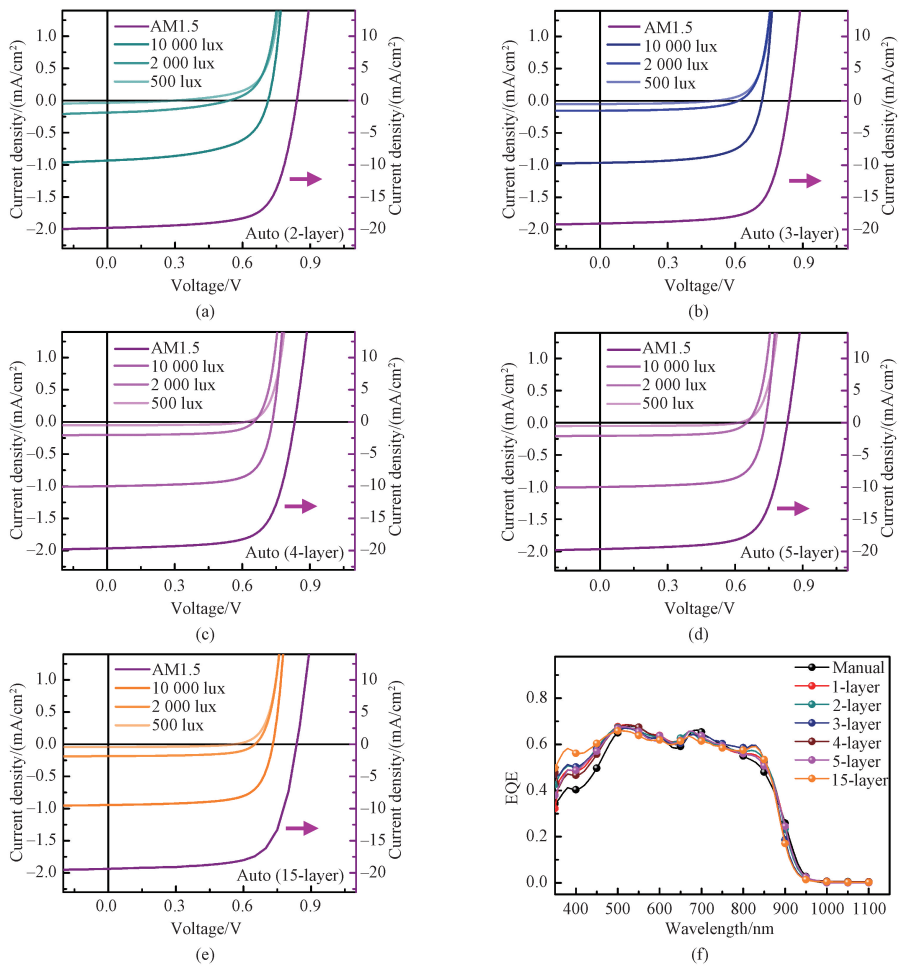

Fig. 7 Performance characterizations of PM6∶Y6 based OPV devices fabricated via automated spin-coating: *J-V* curves of (a) 2-layer, (b) 3-layer, (c) 4-layer, (d) 5-layer and (e) 15-layer based devices; (f) EQE spectra

To further reduce the J_{leak} of the devices, we increased the number of spin-coatings for the AL. By adjusting the concentration of the PM6∶Y6 solution in chloroform, we obtained 100 nm thick ALs through 3, 4, 5 and 15 spin-coating cycles. The optical microscopy and AFM test results of these ALs are shown in Fig. 4. It can be observed that as the number of spin-coatings increases, the density of pinhole defects in the AL gradually decreases. When the number of spin-coatings reaches 5, pinhole defects are practically not observed. The dark *J-V* curves of the devices fabricated based on the 3-layer, 4-layer, 5-layer and 15-layer ALs are shown in Fig. 5. The statistical analysis of R_{sh} and J_{leak} for 20 sets of devices is summarized in Figs. 6(a) and 6(b). From Fig. 6, we can see that as the number of spin-coatings increases, the dispersion of R_{sh} remains relatively unchanged, but the average value of R_{sh} increases. When the number of spin-coatings reaches five, the R_{sh} of the devices stabilizes, with an average value of approximately 1×10^3 kΩ/cm^2. At this point, the J_{leak} of the devices also stabilizes, at around 1×10^{-3} mA/cm^2. Under LED (6500 K) illumination conditions, even at a low light intensity of 500 lux, the devices still exhibit considerable PCE, approximately 9.72%.

The reason why the sequential deposition process led to reduced density of pinhole defects can be attributed to the following. Due to the high rotational speed during spin-coating, the solvent evaporates rapidly. Since the same solvent is used for each layer deposition, the subsequent deposition of the AL has no destructive effect on the previously deposited layers. In this case, taking the example of the two-time deposition process for the AL, although pinhole defects exist in both the first and second deposition layers, the locations of the pinhole defects differ between these two layers. Furthermore, during the second deposition of the AL, there is a high probability that the pinhole defects in the first layer will be filled by the second layer. Therefore, the two-time deposition can effectively reduce the density of pinholes that can penetrate the entire AL, thereby reducing the likelihood of contact between the cathode and anode in the OPV device, improving R_{sh} and decreasing J_{leak}.

To confirm that the sequential deposition process did not cause damage to the previously deposited ALs, we conducted an experiment by depositing a layer of active material on a glass substrate and then using the same spin-coating conditions to spin-coat pure chloroform solvent without the active materials. The surface profilometer measurements revealed that after spin-coating the pure solvent, the thickness of the AL remained almost unchanged, and the density of pinhole defects in the AL did not change (Fig. 8).

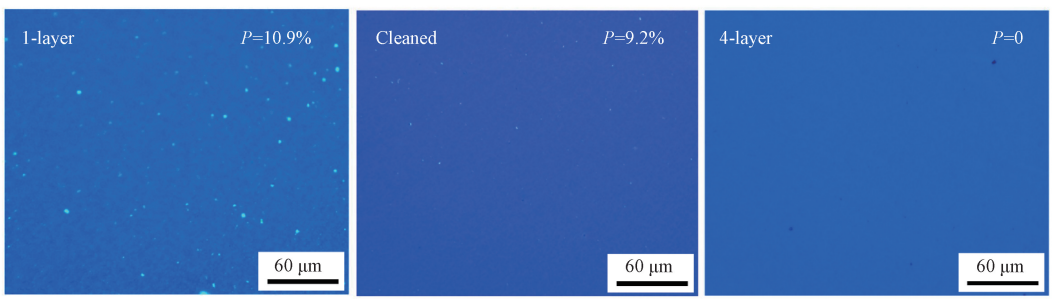

Fig. 8 Reflectance images of PM6∶Y6 AL thin films with different layers by automated spin-coating: (a) 1-layer; (b) following a cleaning step involving pure chloroform applied on top of the film from (a); (c) 4-layer

3 Conclusions

In this study, we investigated leakage currents in OPV devices, which hindered their performance under indoor illumination conditions. The high density of pinhole defects in the AL fabricated from a solution was identified as the root cause of these elevated leakage currents. By combining an automated spin-coating strategy with sequential deposition processes, the compactness of the AL was significantly enhanced, and the density of pinhole defects within it was mitigated. Our findings demonstrated that as the number of deposition cycles increased, the density of pinhole defects in the AL notably decreased. Beyond three deposition cycles, pinhole defects were virtually absent in the AL, resulting in an escalating R_{sh} in correlation with the number of depositions. As a result, the automated sequential deposition strategy substantially enhanced device performance under weak indoor light conditions. Specifically, for OPV devices based on PM6∶Y6, evaluated under 6500 K LED illumination at an intensity of 10000 lux, the PCE derived from a single spin-coating process only reached 8.41%. In contrast, the PCE of devices with the AL coated via five depositions escalated to 15.57%. These results underscore the crucial role of AL processing conditions in curbing device leakage current, ultimately amplifying the performance of indoor OPV devices.

References

[1] HEEGER A J. 25th anniversary article: bulk heterojunction solar cells: understanding the mechanism of operation [J]. *Advanced Materials*, 2014, 26(1): 10-27.

[2] SPANGGAARD H, KREBS F C. A brief history of the development of organic and polymeric photovoltaics[J]. *Solar Energy Materials and Solar Cells*, 2004, 83(2/3): 125-146.

[3] LIU Y H, LIU B W, MA C Q, et al. Recent progress in organic solar cells (Part I material science)[J]. *Science China Chemistry*, 2022, 65(2): 224-268.

[4] LIU Y H, LIU B W, MA C Q, et al. Recent progress in organic solar cells (Part II device engineering)[J]. *Science China Chemistry*, 2022, 65(8): 1457-1497.

[5] CHEN L X. Organic solar cells: recent progress and challenges[J]. *ACS Energy Letters*, 2019, 4(10): 2537-2539.

[6] SUN Y N, LIU T, KAN Y Y, et al. Flexible organic solar cells: progress and challenges[J]. *Small Science*, 2021, 1(5): 2100001.

[7] SUN L C, CHEN Y C, SUN M T, et al. Organic solar cells: physical principle and recent advances[J]. *Chemistry, an Asian Journal*, 2023, 18(5): e202300006.

[8] GUO Y Q, HUANG J, LI Z, et al. Design and synthesis of acceptor-donor-acceptor type non-fullerene acceptors using oxindole-based bridge for polymer solar cells applications[J]. *Journal of Donghua University (English Edition)*, 2022, 39(3): 272-280.

[9] SHOCKLEY W, QUEISSER H J. Detailed balance limit of efficiency of p-n junction solar cells[J]. *Journal of Applied Physics*, 1961, 32(3): 510-519.

[10] HO J K W, YIN H, SO S K. From 33% to 57%: an elevated potential of efficiency limit for indoor photovoltaics[J]. *Journal of Materials Chemistry A*, 2020, 8(4): 1717-1723.

[11] CUI Y, WANG Y M, BERGQVIST J, et al. Wide-gap non-fullerene acceptor enabling high-performance organic photovoltaic cells for indoor applications[J]. *Nature Energy*, 2019, 4: 768-775.

[12] CUTTING C L, BAG M, VENKATARAMAN D. Indoor light recycling: a new home for organic photovoltaics[J]. *Journal of Materials Chemistry C*, 2016, 4(43): 10367-10370.

[13] JAHANDAR M, KIM S, LIM D C. Indoor organic photovoltaics for self-sustaining IoT devices: progress, challenges and practicalization [J]. *ChemSusChem*, 2021, 14(17): 3449-3474.

[14] XIE L, SONG W, GE J F, et al. Recent progress of organic photovoltaics for indoor energy harvesting[J]. *Nano Energy*, 2021, 82: 105770.

[15] LEE H K H, WU J Y, BARBÉ J, et al. Organic photovoltaic cells: promising indoor light harvesters for self-sustainable electronics [J]. *Journal of Materials Chemistry A*, 2018, 6(14): 5618-5626.

[16] LI B X, HOU B, AMARATUNGA G A J. Indoor photovoltaics, the next big trend in solution-processed solar cells [J]. *InfoMat*, 2021, 3(5): 445-459.

[17] CHEN Z H, YIN H, WEN Z C, et al. Organic indoor light harvesters achieving recorded output power over 500% enhancement under thermal radiated illuminances [J]. *Science Bulletin*, 2021, 66(16): 1641-1648.

[18] STEIM R, AMERI T, SCHILINSKY P, et al. Organic photovoltaics for low light applications [J]. *Solar Energy Materials and Solar Cells*, 2011, 95(12): 3256-3261.

[19] CUI Y, HONG L, HOU J H. Organic photovoltaic cells for indoor applications: opportunities and challenges[J]. *ACS Applied Materials & Interfaces*, 2020, 12(35): 38815-38828.

[20] RYU H S, PARK S Y, LEE T H, et al. Recent progress in indoor organic photovoltaics [J]. *Nanoscale*, 2020, 12(10): 5792-5804.

[21] DU B L, YANG R Z, HE Y Z, et al. Nondestructive inspection, testing and evaluation for Si-based, thin film and multi-junction solar cells: an overview [J]. *Renewable and Sustainable Energy Reviews*, 2017, 78: 1117-1151.

[22] LI M, ZHAO C, WANG Z K, et al. Interface modification by ionic liquid: a promising candidate for indoor light harvesting and stability improvement of planar perovskite solar cells[J]. *Advanced Energy Materials*, 2018, 8(24): 1801509.

[23] JAIN S C, KAPOOR A K, GEENS W, et al. Trap filled limit of conducting organic materials [J]. *Journal of Applied Physics*, 2002, 92(7): 3752-3754.

[24] SAEED M A, KIM S H, KIM H, et al. Indoor organic photovoltaics: optimal cell design principles with synergistic parasitic resistance and optical modulation effect[J]. *Advanced Energy Materials*, 2021, 11(27): 2003103.

[25] MORI S, GOTANDA T, NAKANO Y, et al. Investigation of the organic solar cell characteristics for indoor LED light applications [J]. *Japanese Journal of Applied Physics*, 2015, 54(7): 071602.

[26] JE H I, SHIN E Y, LEE K J, et al.

Understanding the performance of organic photovoltaics under indoor and outdoor conditions: effects of chlorination of donor polymers [J]. *ACS Applied Materials & Interfaces*, 2020, 12(20): 23181-23189.
[27] YANG S S, HSIEH Z C, KESHTOV M L, et al. Toward high-performance polymer photovoltaic devices for low-power indoor applications [J]. *Solar RRL*, 2017, 1(12): 1700174.
[28] PARK S Y, LABANTI C, LUKE J, et al. Organic bilayer photovoltaics for efficient indoor light harvesting[J]. *Advanced Energy Materials*, 2022, 12(3): 2103237.
[29] ZHOU X B, WU H B, LIN B J, et al. Different morphology dependence for efficient indoor organic photovoltaics: the role of the leakage current and recombination losses [J]. *ACS Applied Materials & Interfaces*, 2021, 13(37): 44604-44614.
[30] ZHOU X B, WU H B, BOTHRA U, et al. Over 31% efficient indoor organic photovoltaics enabled by simultaneously reduced trap-assisted recombination and non-radiative recombination voltage loss[J]. *Materials Horizons*, 2023, 10(2): 566-575.
[31] PROCTOR C M, NGUYEN T Q. Effect of leakage current and shunt resistance on the light intensity dependence of organic solar cells [J]. *Applied Physics Letters*, 2015, 106(8): 083301.
[32] MATHEWS I, KANTAREDDY S N, BUONASSISI T, et al. Technology and market perspective for indoor photovoltaic cells [J]. *Joule*, 2019, 3(6): 1415-1426.
[33] BURWELL G, SANDBERG O J, LI W, et al. Scaling considerations for organic photovoltaics for indoor applications[J]. *Solar RRL*, 2022, 6(7): 2200315.
[34] ZHANG M J, GUO X, MA W, et al. A large-bandgap conjugated polymer for versatile photovoltaic applications with high performance [J]. *Advanced Materials*, 2015, 27(31): 4655-4660.
[35] YUAN J, ZHANG Y Q, ZHOU L Y, et al. Single-junction organic solar cell with over 15% efficiency using fused-ring acceptor with electron-deficient core [J]. *Joule*, 2019, 3(4): 1140-1151.
[36] TANG Z, ANDERSSON L M, GEORGE Z, et al. Interlayer for modified cathode in highly efficient inverted ITO-free organic solar cells[J]. *Advanced Materials*, 2012, 24(4): 554-558.

降低漏电流并提升室内有机光伏器件光伏性能

王 翔, 高佳欣, 李 正, 王 明*, 唐 正*
东华大学 先进低维材料中心, 材料科学与工程学院, 纤维材料改性国家重点实验室, 上海 201620

摘 要: 有机光伏 (organic photovoltaic, OPV) 器件在室内光采集方面前景广阔, 其功率转换效率的理论上限超过了其他光伏技术。然而, OPV 器件中高漏电流的存在通常会限制其在室内条件下的有效性能。该研究证实了 OPV 器件中高漏电流的起源在于薄膜层内存在的针孔缺陷。将自动旋涂策略与顺序沉积工艺相结合, 显著提高了活性层的紧凑性, 并将针孔缺陷的发生降至最低。试验结果表明, 随着沉积循环次数的增加, 活性层中针孔缺陷的密度显著降低, 因而漏电流显著降低了几个数量级。这是通过不断优化活化层沉积工艺而实现的。这使 OPV 器件在室内照明条件下的功率转换效率提高了两倍。

关键词: 有机光伏 (OPV); 室内光采集; 针孔缺陷; 漏电流; 分流电阻